CHEMISTRY OF MATERIALS

Article

pubs.acs.org/cm

Sub-micron Polymer–Zeolitic Imidazolate Framework Layered Hybrids via Controlled Chemical Transformation of Naked ZnO Nanocrystal Films

Stephen M. Meckler,[†,⊥] Changyi Li,[‡,⊥] Wendy L. Queen,[⊥,○] Teresa E. Williams,[§,⊥] Jeffrey R. Long,[†,∥] Raffaella Buonsanti,[∥,▽] Delia J. Milliron,[■] and Brett A. Helms*[,⊥,∥]

[†]Department of Chemistry, [‡]Department of Chemical and Biomolecular Engineering, and [§]Graduate Group in Applied Science and Technology, University of California, Berkeley, California 94720, United States

[⊥]The Molecular Foundry, [∥]Materials Science Division, and [▽]Joint Center for Artificial Photosynthesis, Lawrence Berkeley National Laboratory, Berkeley, California 94720, United States

[○]Department Institut des Sciences et Ingénierie Chimiques, École Polytechnique Fédérale de Lausanne (EPFL), CH 1051 Sion, Switzerland

[■]McKetta Department of Chemical Engineering, The University of Texas at Austin, Austin, Texas 78712, United States

Supporting Information

ABSTRACT: Here we show that sub-micron coatings of zeolitic imidazolate frameworks (ZIFs) and even ZIF–ZIF bilayers can be grown directly on polymers of intrinsic microporosity from zinc oxide (ZnO) nanocrystal precursor films, yielding a new class of all-microporous layered hybrids. The ZnO-to-ZIF chemical transformation proceeded in less than 30 min under microwave conditions using a solution of the imidazole ligand in *N*,*N*-dimethylformamide (DMF), water, or mixtures thereof. By varying the ratio of DMF to water, it was possible to control the morphology of the ZIF-on-polymer from isolated crystallites to continuous films. Grazing incidence X-ray diffraction was used to confirm the presence of crystalline ZIF in the thin films, and X-ray absorption spectroscopy was used to quantify film purity, revealing films with little to no residual ZnO. The role solvent plays in the transformation mechanism is discussed in light of these findings, which suggest the ZnO nanocrystals may be necessary to localize heterogeneous nucleation of the ZIF to the polymer surface.

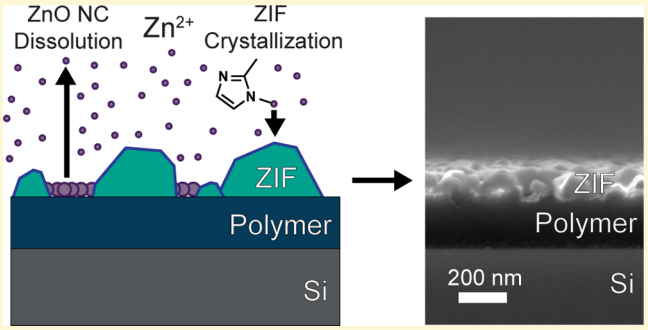

INTRODUCTION

A hybrid material can exhibit functional properties greater than the sum of its parts when its components are chosen and arranged rationally.[1,2] Assembling such a composite requires attention to the chemistry, size, and morphology of each component. Furthermore, controlling composite architecture necessitates consideration of the interfaces between these components. While there are many examples of functional composites with a dispersed phase in a host matrix (e.g., mechanically reinforced polymer composites,[3−5] composite electrodes for electrochemical devices,[6,7] and switchable photonic displays[8,9]), those with layered architectures are fewer and are often more difficult to fabricate. This is the case with ZIF–polymer composites, where producing layered composites is more time-consuming and less controllable than the formation of mixed-matrix composites.[10−14]

Here we show that sub-micron-thick ZIF films can be grown in a controllable manner via a ZnO-to-ZIF dissolution–crystallization scheme carried out on polymers of intrinsic microporosity (PIMs), yielding layered microporous composites for the first time (Figure 1). ZIFs are robust materials demonstrating great promise in a variety of applications including separations, catalysis, sensing, and electronics.[13,15−17] The ultrathin films reported here are especially promising for asymmetric membranes, where thin selective layers provide high selectivity without sacrificing flux. The morphology of these ZIF films on polymer is strongly influenced by the reaction conditions used to convert nanocrystalline ZnO to either ZIF-7 or ZIF-8, highlighting the deterministic role solvent plays on ZnO dissolution as well as ZIF nucleation and growth. The unique layered architecture made possible by these synthetic advances required us to apply synchrotron X-ray techniques to understand the structure and composition of the composite in a quantitative manner. Through the use of these techniques, we were able to directly

Received: August 20, 2015
Revised: October 9, 2015
Published: October 13, 2015

DOI: 10.1021/acs.chemmater.5b03219
Chem. Mater. 2015, 27, 7673−7679

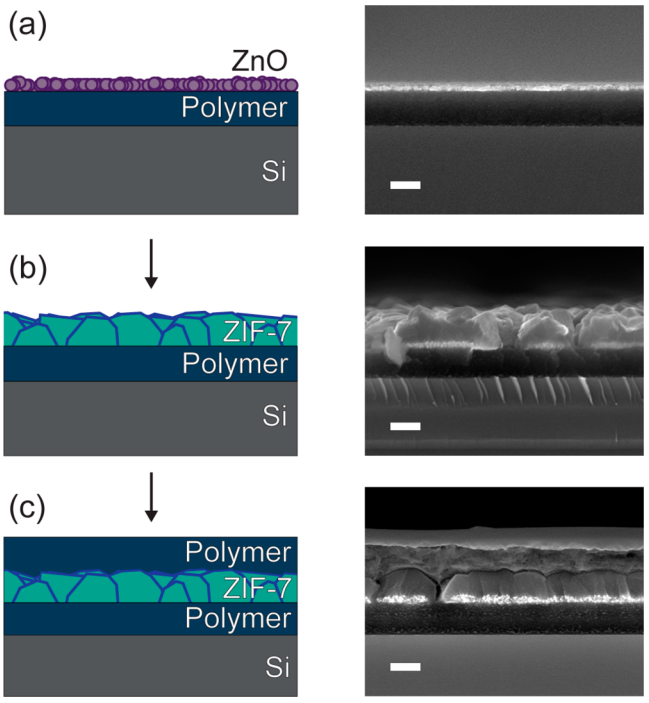

Figure 1. Scheme and cross-sectional SEM images depicting (a) ZnO nanocrystals on a polymer film, (b) a ZIF-7 film grown from sacrificial ZnO nanocrystals, and (c) a PIM/ZIF-7/PIM trilayer structure. Scale bars are 200 nm.

probe the nanoscale ZIF films rather than relying on the products of analogous bulk reactions.

Our implementation of cationic naked ZnO nanocrystals as precursors to sub-micron-thick ZIF films is unique and overcomes several challenges previously encountered with direct growth methods from solution-phase precursors. In those cases, ZIF films with thicknesses of microns or even tens of microns are more common.[10,12,18−22] Thinner films, which help shorten molecular diffusion paths, generally require multistep layer-by-layer strategies (e.g., SURMOFs), and while 100 nm ZIF-8 films have been grown solvothermally on glass and silicon, extending this technique to polymers frequently requires substrate modification.[19,23−27] In the present scheme, we limit the total Zn(II) available for ZIF formation simply by controlling the ZnO nanocrystal film thickness, and as the ZIF growth is directed by the ZnO nanocrystal layer, no functionalization of the polymer is necessary. We also hypothesize that the high surface area inherent to these 0D nanostructures aids in conversion rate and efficacy. In that regard, our results are complementary to previous work reporting ZIF growth on nanoscopic ZnO and $Zn(OH)_2$ materials, which have been transformed into both 1D and 2D ZnO−ZIF or $Zn(OH)_2$−ZIF hybrids.[28−37] Metal oxides and hydroxides have also been used to grow other classes of porous crystals, including metal−organic frameworks (MOFs) via pseudomorphic replication.[38,39] Common to these schemes is the etching of the metal oxide or hydroxide by the ligand (i.e., dissolution) and subsequent nucleation and growth of the framework material (i.e., crystallization).

RESULTS AND DISCUSSION

We found that the conversion of cationic naked ZnO nanocrystal films (15−30 nm thick) to either ZIF-7 or ZIF-8 coatings (100−500 nm thick) on cross-linked films of PIM-1 (~200 nm thick) proceeded readily using a low-temperature microwave reaction (Figure 1a,b). Typically, ~7 nm ZnO nanocrystals were spin-coated on a cross-linked polymer film atop a silicon substrate. The nanocrystal-coated polymer film was submerged facedown in a solution of either benzimidazole or 2-methylimidazole in a water/DMF mixture ($[\text{imidazole ligand}]_0$ = 1.11 M) to induce transformation to ZIF-7 or ZIF-8, respectively. The vessel was subjected to microwave radiation without stirring to maintain an internal solution temperature of 50 °C for 30 min. Substrates were then retrieved and washed by dipping in a solvent bath (DMF for ZIF-7 films; deionized water for ZIF-8 films) to remove excess ligand. A sandwich structure with the ZIF between two layers of polymer was generated by spin-coating another layer of PIM-1 over the ZIF surface (Figure 1c). Unusual ZIF-8/ZIF-7 multilayers could also be prepared on cross-linked PIM-1 films through the sequential deposition and transformation of ZnO nanocrystal films with 2-methylimidazole and benzimidazole in turn (Figure S1 of the Supporting Information). Notably, in no cases was surface modification of PIM-1 necessary to adhere the ZnO nanocrystals or ZIF films, where in previous work, amine functionalization of the polymer was needed to promote heterogeneous nucleation and adhesion of the ZIF.[27]

Cross-sectional and top-down SEM were used to study the resultant film morphology. Contrast differences between residual ZnO nanocrystals and the overlying ZIF made each phase readily distinguishable. Crystalline ZIF-7 or ZIF-8 within the layered hybrid was detected using powder X-ray diffraction (PXRD) and synchrotron grazing incidence X-ray diffraction (GIXD) (Figure 2). GIXD patterns provided high signal-to-noise crystallographic identification with increased surface sensitivity, mitigating the overwhelming baseline from the amorphous polymer seen in the PXRD data.[40] This allowed us to directly collect diffraction patterns of ZIF on the polymer films. The 2D GIXD patterns were isotropic, revealing no preferential ZIF orientation with respect to the plane of the film (Figure S2). To provide further insight into the fundamental steps in the present scheme, we explored in greater detail the reaction conditions that influenced ZIF film formation on PIM-coated substrates.

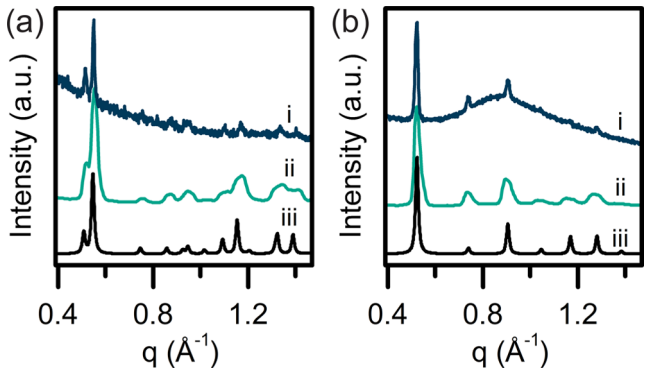

Figure 2. Diffraction patterns of (a) ZIF-7 and (b) ZIF-8 thin films on PIM-1 polymer supports, including (i) PXRD, (ii) GIXD, and (iii) simulated diffraction patterns.

Our systematic investigation of the reaction conditions used for the ZnO-to-ZIF-8 film transformation revealed significant control over film thickness and grain size with changes to the reaction solvent: here, mixtures of water and DMF (Figure 3). Other reaction parameters, including temperature, ligand

DOI: 10.1021/acs.chemmater.5b03219
Chem. Mater. 2015, 27, 7673−7679

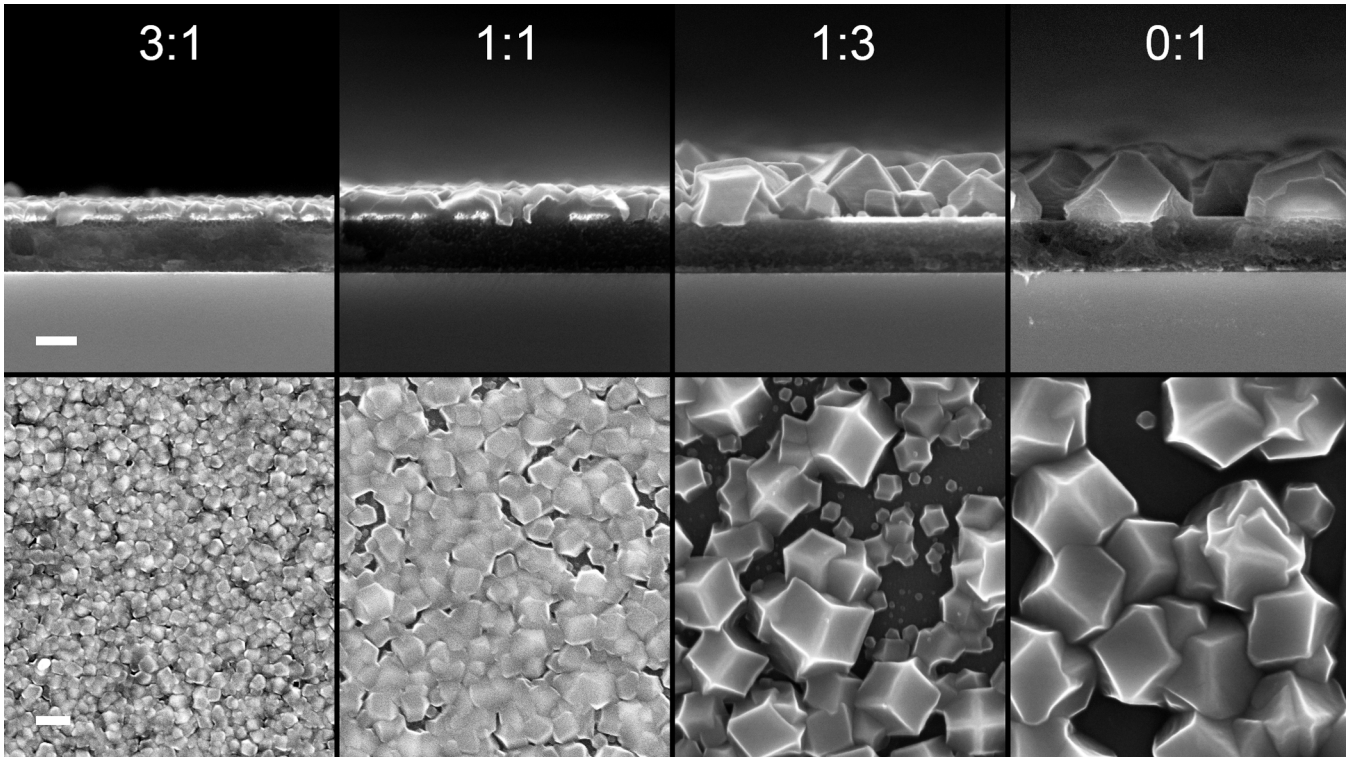

Figure 3. SEM images of ZIF-8 coatings transformed from 30 nm thick sacrificial ZnO films at various DMF:water (v/v) ratios. Both cross-sectional (top row) and top-down (bottom row) views are shown. Scale bars are 200 nm.

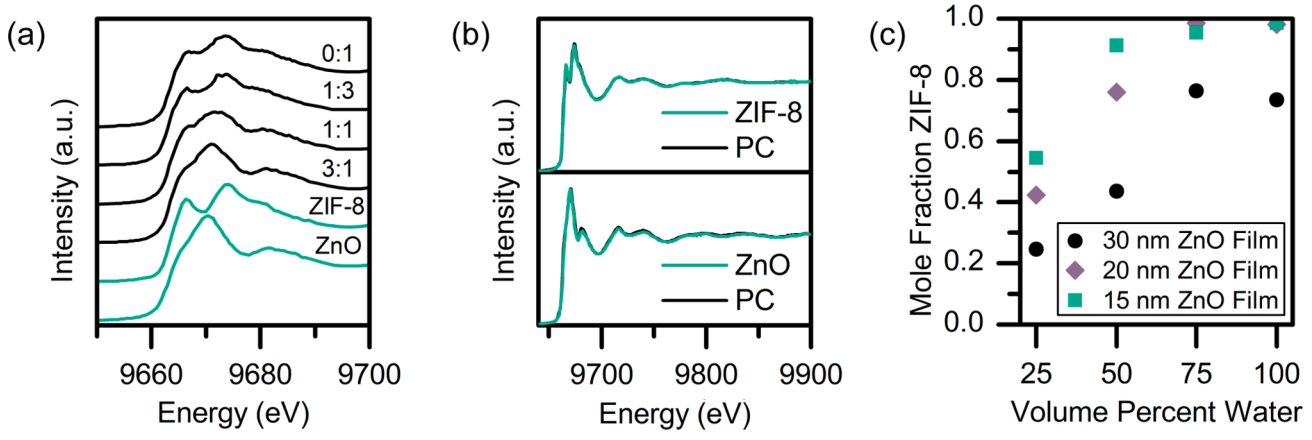

Figure 4. Quantitative XANES characterization of ZIF-8 films transformed from ZnO coatings at various DMF:water (v/v) ratios. (a) Spectra of bulk ZnO and ZIF-8 (green) and of ZIF-8 films (black). (b) The two principal components (PC) best expressing change in the experimental data set (black) match experimentally collected bulk ZIF-8 and ZnO spectra (green). (c) Mole fraction of Zn in ZIF-8 after the chemical transformation of ZnO nanocrystal films (average film thickness = 15 nm, 20 nm, or 30 nm) using different solvent mixtures. These data can be taken as a measure of film purity with respect to ZIF and residual ZnO.

concentration, and reaction time, were investigated but failed to both provide control over ZIF film growth and produce high-quality coatings. Transformations employing reaction mixtures up to 50 vol % water yielded comparatively smooth, continuous ZIF-8 films as thick as ~150 nm. The continuous nature of the films produced under these reaction conditions suggests the formation of many ZIF-8 nuclei and comparatively slow crystal growth. Unincorporated Zn(II) is presumed to be lost to solution or retained as residual ZnO trapped at the ZIF–polymer interface. If all the ZnO were successfully transformed, a 30 nm nanocrystal layer would produce a ~320 nm thick ZIF-8 film.[41] As the water content of the reaction mixture increased beyond 50 vol %, significantly less ZnO was visible in the cross-sectional SEM images and the ZIF-8 grain size increased. In these cases, the ZIF-8 coatings ceased to be continuous; instead, the growth of faceted, isolated crystals adhered to the polymer surface was observed. Reducing the thickness of the sacrificial ZnO layer only slightly changed the morphology of the ZIF coatings but resulted in significantly less residual ZnO in the SEM cross sections (Figures S3–S4). ZnO nanocrystal film thicknesses were controlled by diluting the dispersion from which the films were cast, and approximate ZnO film thicknesses were measured using cross-sectional SEM (Figure S5). ZIF-8 coatings formed from even the thinnest ZnO

DOI: 10.1021/acs.chemmater.5b03219
Chem. Mater. 2015, 27, 7673–7679

precursor films fabricated. In most cases, the equilibrium rhombic dodecahedral ZIF-8 crystal morphology was observed rather than the kinetically favored cubic morphology.[42] Reactions in pure DMF were not reproducible, which we attribute to the ease with which naked ZnO nanocrystals redisperse in this solvent. As benzimidazole is sparingly soluble in water, an analogous study of the ZnO-to-ZIF-7 transformation is not included here.

To quantify the purity of ZIF-8 layers produced in different solvent mixtures (i.e., with respect to any residual ZnO), X-ray absorption near-edge structure (XANES) spectra of representative samples produced in four DMF:water mixtures were compared to reference spectra for ZnO nanocrystals and ZIF-8. XANES total fluorescence yield spectra of the Zn K-edge are well-suited to the analysis of our hybrid films: they are unaffected by the presence of the underlying PIM-1 film; the probe depth is micron scale; and the fluorescence intensites of Zn atoms in different electronic environments, here ZIF-8 and ZnO, are the same (see Experimental Section for more information). XANES spectra were collected from each sample at multiple spots near the center of the film and averaged together to faithfully represent the sample composition and to reduce beam damage on the ZIF-8 (Figure 4a). Principal component analysis (PCA) was performed on the data set. The two principal components best expressing change in the data set were compared against reference spectra taken of ZIF-8 and ZnO (Figure 4b). Both exhibit excellent agreement, suggesting the Zn content of the films can be accurately modeled as a mixture of only ZIF-8 and ZnO. Least-squares fits of the reference spectra to each experimental film provided a quantitative fraction of the total Zn present in each crystalline phase (Figure 4c). The XANES fits reveal that as the volume fraction of water in the reaction medium increases and the thickness of the ZnO precursor film decreases, the films tend toward pure ZIF-8, which is in good agreement with the phenomenological interpretation of the SEM cross sections. Continuous, nearly pure ZIF-8 coatings were obtained from 15 nm thick ZnO films transformed in 50 vol % water solutions (Figure 5). To demonstrate the reproducibility of sample preparation, the experiment was repeated for the 30 nm thick ZnO films three times, and in no case was the standard error greater than 8 mol % (Figure S6).

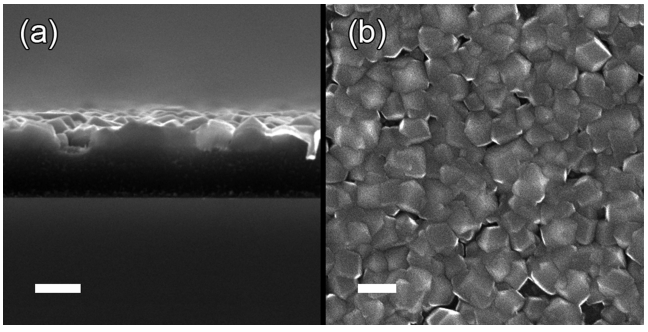

Figure 5. (a) Cross-sectional SEM image of a ZIF-8 coating on PIM that is >90% pure with respect to residual ZnO. (b) Top-down image of the same film shows significant surface coverage. Scale bars are 200 nm.

While several metal oxide-to-MOF chemical transformations have been reported in the literature, the mechanism of this chemical conversion is still under investigation. Different metal oxide/ligand pairs and the conditions in which the reaction is carried out may change the mechanism of MOF formation.[30,38] Clearly, the metal oxide-to-MOF conversion depends on the competing rates of several processes: (1) metal oxide dissolution, (2) metal-ion diffusion away from the polymer surface, (3) MOF nucleation (possibly from an amorphous precursor), (4) MOF growth, and (5) Ostwald ripening (Figure S7). The relative rates of these processes dictate the overall kinetics of the reaction and the resultant morphology and composition of the product.

In the scheme presented here, water and DMF each affect these competing rates. The transforming solutions show an increase in pH with increasing water content, from pH 9 at 25 vol % water to pH 11 at 100 vol % water. Increasing the vol % of water therefore results in faster etching of the amphoteric ZnO, increased proton mobility overall, and more facile deprotonation of the ZIF crystal surfaces, which in turn promotes crystal growth over nucleation of new crystallites.[43] DMF, aside from regulating etching by modulating pH, may also be responsible for inhibiting ZIF growth as has been reported in some solvothermal ZIF-8 syntheses.[44] Finally, we considered whether differences in microwave absorption might affect the energy available to the system. However, since water and DMF have similar loss tangent values, both solvents can be expected to behave similarly under microwave radiation.[45]

As ZnO has been reported previously as an effective templating agent for the solvothermal growth of ZIF films, we reasoned that metal oxide may be necessary for a local ZIF nucleation event, consistent with a heterogeneous nucleation mechanism.[11,36,46] Phase-pure ZIF at the polymer surface was not measured in any of the XANES experiments when the initial ZnO film thickness was 30 nm. If ZnO is needed for heterogeneous nucleation, the voids between crystals due to rapid nanocrystal dissolution are concomitant with fewer nucleation sites in those regions on PIM-1. This is consistent with our observation that voids account for greater fractions of the surface area in films formed using high water content solutions, where ZnO dissolution is more rapid. ZIF coatings transformed from thinner ZnO films produced nearly pure ZIF-8 coatings, which may result from ZIF nucleation occurring directly at the polymer surface, presumably at the nitrile groups decorating the PIM-1 backbone.[47] However, we believe it is more likely the ZIF preferentially nucleates on ZnO nanocrystals that are subsequently etched via diffusion through the ZIF pores, a phenomenon previously reported in similar chemical conversions.[31]

Finally, studying the time-evolution of ZIF-8 film growth in a 75 vol % water solution provided further insight into the contributing and competing influences of ZIF-8 nucleation, growth, and Ostwald ripening (Figure S8). Large crystals, seen in films grown from 75 vol % or pure water solutions, form when nucleation is slow relative to crystal growth. Nucleation occurs as long as ZnO is exposed to the solution, and crystal growth stops when all accessible Zn(II) is depleted, explaining the increased ZIF-8 polydispersity observed in reactions with a high water content. After microwave irradiation for 10 min, few nucleation sites have formed and the surface is primarily ZnO. By 30 min, the surface ZnO is either lost to solution, converted into ZIF-8, or covered by ZIF-8. The crystal size is static over longer reaction times, demonstrating that Ostwald ripening is likely not a significant factor in film formation and that the 30 min reaction time is sufficient to obtain the final film morphology.

DOI: 10.1021/acs.chemmater.5b03219
Chem. Mater. 2015, 27, 7673−7679

CONCLUSION

Sub-micron ZIF-7 and ZIF-8 coatings and bilayers on microporous polymer substrates were obtained through the chemical conversion of naked ZnO nanocrystal precursor films. The high surface area of the nanocrystal films facilitated a rapid conversion under mild conditions to ZIF coatings with morphologies that were controlled by choice of solvent. Crystal structures were confirmed by GIXD, and the morphology and chemical composition of the ZIF-8 films formed under varying reaction conditions were measured using SEM and XANES spectroscopy, respectively. Sub-micron-thick ZIF films encased on both sides by polymer and ZIF-8/ZIF-7 multilayers were accessible, demonstrating an attractive and versatile new methodology to fabricate layered composite architectures. These composite architectures may be well suited to applications in selective separations and sensing. In that the deposition of metal oxide nanocrystals within or on other materials is foreseeable, our techniques may also be applicable to ZIF−polymer composites in a variety of porous polymer formats, including hollow polymer fibers, polymer monoliths, polymer membranes, and polymer beads. Our unique access to ZIF-on-ZIF multilayers likewise suggests new avenues for selective species transport.

EXPERIMENTAL SECTION

Grazing Incidence X-ray Diffraction. GIXD was performed at two beamlines. Data were collected at the Stanford Synchrotron Radiation Laboratory (SSRL) beamline 11-3 with a photon energy of 12.7 keV. A MAR345 2D detector was used at a sample−detector distance of 175 mm. Integration of the diffraction peak areas was performed with the software WxDiff.[48] Additional data were collected at beamline 7.3.3 of the Advanced Light Source, Lawrence Berkeley National Laboratory, using a photon energy of 10 keV, a sample−detector distance of 280 mm, and a Pilatus 2 M detector.[49] These diffraction peak areas were integrated with the software package Nika for Igor Pro.[50] The incident angle at both beamlines was fixed at 0.12° and all experiments were conducted in a He atmosphere. Diffraction patterns were scaled for clarity.

X-ray Absorption Near-Edge Structure Spectroscopy. Zn K-edge XANES spectra were collected at the Advanced Light Source (ALS) beamline 10.3.2.[51] The incident angle was ∼15° and the spot size ∼50 × 3 μm. Scans were taken at between 4 and 20 spots on each sample, until adequate signal to noise was achieved, from 9.56 to 10.00 keV using a Canberra 7-element UltraLEGe solid-state Ge detector or Amp-Tek silicon drift diode detector and averaged together. Spectra of bulk ZnO and ZIF-8 nanocrystals were used in least-squares linear fits of each sample. Monochromator drift was accounted for by making E0 a parameter of the fit. Probe depths were estimated using the Hephaestus software package. At the 15° incident angle used, these depths correspond to a 22.5 μm thick ZIF-8 sample, assuming a density of 1.45 g cm^{-3}, and a 2.14 μm thick ZnO sample, assuming a density of 5.61 g cm^{-3}.[52,53] Because the measured sample thicknesses were well below this limit, no overabsorption correction was used. PCA and least-squares fits were performed on the data set using routines previously described.[54,55,56] These analyses and all other data processing were completed using software provided at the beamline.

ASSOCIATED CONTENT

Supporting Information

Materials, experimental methods, and Figures S1−S10 detailing ZIF-on-ZIF bilayer architectures on PIM-1, GIXD, ZIF-8 film morphology with changes to ZnO film thickness and reaction conditions, ZnO precursor film thicknesses, reproducibility of sample fabrication by XANES, mechanistic considerations of dissolution−crystallization, ZIF-8 growth kinetics on PIM-1, areal views of ZIF film uniformity, ZnO nanocrystal characterization, and PXRD of the ZIF-8 reference standard. The Supporting Information is available free of charge on the ACS Publications website at DOI: 10.1021/acs.chemmater.5b03219.

AUTHOR INFORMATION

Corresponding Author

*E-mail: bahelms@lbl.gov (B.A.H.).

Author Contributions

The manuscript was written through contributions of all authors. All authors have given approval to the final version of the manuscript.

Notes

The authors declare no competing financial interest.

ACKNOWLEDGMENTS

We thank C. Zhu, T. Dunn, and C. Miller for assistance with GIXD; M. Marcus for assistance with XANES; L. Maserati for the ZIF-8 spectral reference sample; and S. Doris and A. Wills for useful discussions. This work was supported as part of the Center for Gas Separations Relevant to Clean Energy Technologies, an Energy Frontier Research Center funded by the U.S. Department of Energy, Office of Science, Basic Energy Sciences, under Award No. SC0001015. Portions of this work, including synthesis, characterization, and chemical transformations thereof, were carried out as User Projects at the Molecular Foundry, which is supported by the Office of Science, Office of Basic Energy Sciences, of the U.S. Department of Energy under Contract No. DE-AC02-05CH11231. XANES spectroscopy and GIXD were carried out at beamlines 10.3.2 and 7.3.3, respectively, of the Advanced Light Source, which is supported by the Director, Office of Science, Office of Basic Energy Sciences, of the U.S. Department of Energy under the same contract. Additional GIXD was carried out at beamline 11-3 at the Stanford Synchrotron Radiation Lightsource, SLAC National Accelerator Laboratory, which is supported by the U.S. Department of Energy, Office of Science, Office of Basic Energy Sciences under Contract No. DE-AC02-76SF00515.

REFERENCES

(1) Sanchez, C.; Julián, B.; Belleville, P.; Popall, M. Applications of Hybrid Organic−Inorganic Nanocomposites. *J. Mater. Chem.* **2005**, *15*, 3559−3592.

(2) Thompson, R. B.; Ginzburg, V. V.; Matsen, M. W.; Balazs, A. C. Predicting the Mesophases of Copolymer-Nanoparticle Composites. *Science* **2001**, *292*, 2469−2472.

(3) Coleman, J. N.; Khan, U.; Blau, W. J.; Gun'ko, Y. K. Small but Strong: A Review of the Mechanical Properties of Carbon Nanotube-Polymer Composites. *Carbon* **2006**, *44*, 1624−1652.

(4) Bauer, J.; Hengsbach, S.; Tesari, I.; Schwaiger, R.; Kraft, O. High-Strength Cellular Ceramic Composites with 3D Microarchitecture. *Proc. Natl. Acad. Sci. U. S. A.* **2014**, *111*, 2453−2458.

(5) Liff, S. M.; Kumar, N.; McKinley, G. H. High-Performance Elastomeric Nanocomposites via Solvent-Exchange Processing. *Nat. Mater.* **2007**, *6*, 76−83.

(6) Aricò, A. S.; Bruce, P.; Scrosati, B.; Tarascon, J.-M.; van Schalkwijk, W. Nanostructured Materials for Advanced Energy Conversion and Storage Devices. *Nat. Mater.* **2005**, *4*, 366−377.

(7) Kim, J.; Ong, G. K.; Wang, Y.; LeBlanc, G.; Williams, T. E.; Mattox, T. M.; Helms, B. A.; Milliron, D. J. Nanocomposite Architecture for Rapid, Spectrally-Selective Electrochromic Modulation of Solar Transmittance. *Nano Lett.* **2015**, *15*, 5574−5579.

DOI: 10.1021/acs.chemmater.5b03219
Chem. Mater. 2015, 27, 7673−7679

(8) Arsenault, A. C.; Míguez, H.; Kitaev, V.; Ozin, G. A.; Manners, I. A Polychromic, Fast Response Metallopolymer Gel Photonic Crystal with Solvent and Redox Tunability: A Step Towards Photonic Ink (P-Ink). *Adv. Mater.* **2003**, *15*, 503−507.
(9) Arsenault, A. C.; Puzzo, D. P.; Manners, I.; Ozin, G. A. Photonic-Crystal Full-Colour Displays. *Nat. Photonics* **2007**, *1*, 468−472.
(10) Brown, A. J.; Brunelli, N. A.; Eum, K.; Rashidi, F.; Johnson, J. R.; Koros, W. J.; Jones, C. W.; Nair, S. Interfacial Microfluidic Processing of Metal-Organic Framework Hollow Fiber Membranes. *Science* **2014**, *345*, 72−75.
(11) Li, W.; Meng, Q.; Li, X.; Zhang, C.; Fan, Z.; Zhang, G. Non-Activation ZnO Array as a Buffering Layer to Fabricate Strongly Adhesive Metal-Organic Framework/PVDF Hollow Fiber Membranes. *Chem. Commun.* **2014**, *50*, 9711−9713.
(12) Yao, J.; Dong, D.; Li, D.; He, L.; Xu, G.; Wang, H. Contra-Diffusion Synthesis of ZIF-8 Films on a Polymer Substrate. *Chem. Commun.* **2011**, *47*, 2559−2561.
(13) Chen, B.; Yang, Z.; Zhu, Y.; Xia, Y. Zeolitic Imidazolate Framework Materials: Recent Progress in Synthesis and Applications. *J. Mater. Chem. A* **2014**, *2*, 16811−16831.
(14) Bushell, A. F.; Attfield, M. P.; Mason, C. R.; Budd, P. M.; Yampolskii, Y.; Starannikova, L.; Rebrov, A.; Bazzarelli, F.; Bernardo, P.; Jansen, J. C.; Lanč, M.; Friess, K.; Shantarovich, V.; Gustov, V.; Isaeva, V. Gas Permeation Parameters of Mixed Matrix Membranes Based on the Polymer of Intrinsic Microporosity PIM-1 and the Zeolitic Imidazolate Framework ZIF-8. *J. Membr. Sci.* **2013**, *427*, 48−62.
(15) Park, K. S.; Ni, Z.; Côté, A. P.; Choi, J. Y.; Huang, R.; Uribe-Romo, F. J.; Chae, H. K.; O'Keeffe, M.; Yaghi, O. M. Exceptional Chemical and Thermal Stability of Zeolitic Imidazolate Frameworks. *Proc. Natl. Acad. Sci. U. S. A.* **2006**, *103*, 10186−10191.
(16) Kreno, L. E.; Leong, K.; Farha, O. K.; Allendorf, M.; Van Duyne, R. P.; Hupp, J. T. Metal-Organic Framework Materials as Chemical Sensors. *Chem. Rev.* **2012**, *112*, 1105−1125.
(17) Sorribas, S.; Gorgojo, P.; Téllez, C.; Coronas, J.; Livingston, A. G. High Flux Thin Film Nanocomposite Membranes Based on Metal−Organic Frameworks for Organic Solvent Nanofiltration. *J. Am. Chem. Soc.* **2013**, *135*, 15201−15208.
(18) Huang, X.; Zheng, B.; Liu, Z.; Tan, C.; Liu, J.; Chen, B.; Li, H.; Chen, J.; Zhang, X.; Fan, Z.; Zhang, W.; Guo, Z.; Huo, F.; Yang, Y.; Xie, L.-H.; Huang, W.; Zhang, H. Coating Two-Dimensional Nanomaterials with Metal-Organic Frameworks. *ACS Nano* **2014**, *8*, 8695−8701.
(19) Lu, G.; Hupp, J. T. Metal-Organic Frameworks as Sensors: A ZIF-8 Based Fabry-Pérot Device as a Selective Sensor for Chemical Vapors and Gases. *J. Am. Chem. Soc.* **2010**, *132*, 7832−7833.
(20) Kwon, H. T.; Jeong, H.-K. In Situ Synthesis of Thin Zeolitic-Imidazolate Framework ZIF-8 Membranes Exhibiting Exceptionally High Propylene/Propane Separation. *J. Am. Chem. Soc.* **2013**, *135*, 10763−10768.
(21) Cacho-Bailo, F.; Seoane, B.; Téllez, C.; Coronas, J. ZIF-8 Continuous Membrane on Porous Polysulfone for Hydrogen Separation. *J. Membr. Sci.* **2014**, *464*, 119−126.
(22) Bux, H.; Liang, F.; Li, Y.; Cravillon, J.; Wiebcke, M.; Caro, J. Zeolitic Imidazolate Framework with Molecular Sieving Properties by Microwave-Assisted Solvothermal Synthesis. *J. Am. Chem. Soc.* **2009**, *131*, 16000−16001.
(23) Shekhah, O.; Wang, H.; Zacher, D.; Fischer, R. A.; Wöll, C. Growth Mechanism of Metal-Organic Frameworks: Insights into the Nucleation by Employing a Step-by-Step Route. *Angew. Chem., Int. Ed.* **2009**, *48*, 5038−5041.
(24) Arslan, H. K.; Shekhah, O.; Wohlgemuth, J.; Franzreb, M.; Fischer, R. A.; Wöll, C. High-Throughput Fabrication of Uniform and Homogenous MOF Coatings. *Adv. Funct. Mater.* **2011**, *21*, 4228−4231.
(25) Heinke, L.; Tu, M.; Wannapaiboon, S.; Fischer, R. A.; Wöll, C. Surface-Mounted Metal-Organic Frameworks for Applications in Sensing and Separation. *Microporous Mesoporous Mater.* **2015**, *216*, 200−215.
(26) Lu, G.; Farha, O. K.; Zhang, W.; Huo, F.; Hupp, J. T. Engineering ZIF-8 Thin Films for Hybrid MOF-Based Devices. *Adv. Mater.* **2012**, *24*, 3970−3974.
(27) Shamsaei, E.; Low, Z.-X.; Lin, X.; Mayahi, A.; Liu, H.; Zhang, X.; Liu, J. Z.; Wang, H. Rapid Synthesis of Ultrathin, Defect-Free ZIF-8 Membranes via Chemical Vapour Modification of a Polymeric Support. *Chem. Commun.* **2015**, *51*, 11474−11477.
(28) Yue, Y.; Qiao, Z.-A.; Li, X.; Binder, A. J.; Formo, E.; Pan, Z.; Tian, C.; Bi, Z.; Dai, S. Nanostructured Zeolitic Imidazolate Frameworks Derived from Nanosized Zinc Oxide Precursors. *Cryst. Growth Des.* **2013**, *13*, 1002−1005.
(29) Stassen, I.; Campagnol, N.; Fransaer, J.; Vereecken, P.; De Vos, D.; Ameloot, R. Solvent-Free Synthesis of Supported ZIF-8 Films and Patterns through Transformation of Deposited Zinc Oxide Precursors. *CrystEngComm* **2013**, *15*, 9308−9311.
(30) Li, S.; Zhang, W.; Zhu, Y.; Zhao, Q.; Huo, F. Synthesis of MOFs and Their Composite Structures through Sacrificial-Template Strategy. *Cryst. Growth Des.* **2015**, *15*, 1017−1021.
(31) Zhan, W.-W.; Kuang, Q.; Zhou, J.-Z.; Kong, X.-J.; Xie, Z.-X.; Zheng, L.-S. Semiconductor@Metal−Organic Framework Core−Shell Heterostructures: A Case of ZnO@ZIF-8 Nanorods with Selective Photoelectrochemical Response. *J. Am. Chem. Soc.* **2013**, *135*, 1926−1933.
(32) Yang, J.; Xie, Z.; Yin, H.; Wang, J.; Xu, J.; Wang, J.; Lu, J.; Yin, D.; Zhang, Y. Simultaneous Surface and Pore Structure Modification for Growth of ZIF-8 Membranes on Coarse Macroporous Tube. *Microporous Mesoporous Mater.* **2014**, *198*, 263−270.
(33) Li, J.; Cao, W.; Mao, Y.; Ying, Y.; Sun, L.; Peng, X. Zinc Hydroxide Nanostrands: Unique Precursors for Synthesis of ZIF-8 Thin Membranes Exhibiting High Size-Sieving Ability for Gas Separation. *CrystEngComm* **2014**, *16*, 9788−9791.
(34) Drobek, M.; Bechelany, M.; Vallicari, C.; Abou Chaaya, A.; Charmette, C.; Salvador-Levehang, C.; Miele, P.; Julbe, A. An Innovative Approach for the Preparation of Confined ZIF-8 Membranes by Conversion of ZnO ALD Layers. *J. Membr. Sci.* **2015**, *475*, 39−46.
(35) Khaletskaya, K.; Turner, S.; Tu, M.; Wannapaiboon, S.; Schneemann, A.; Meyer, R.; Ludwig, A.; Van Tendeloo, G.; Fischer, R. A. Self-Directed Localization of ZIF-8 Thin Film Formation by Conversion of ZnO Nanolayers. *Adv. Funct. Mater.* **2014**, *24*, 4804−4811.
(36) Zhang, X.; Liu, Y.; Kong, L.; Liu, H.; Qiu, J.; Han, W.; Weng, L.-T.; Yeung, K. L.; Zhu, W. A Simple and Scalable Method for Preparing Low-Defect ZIF-8 Tubular Membranes. *J. Mater. Chem. A* **2013**, *1*, 10635−10638.
(37) Yue, Y.; Mehio, N.; Binder, A. J.; Dai, S. Synthesis of Metal−Organic Framework Particles and Thin Films via Nanoscopic Metal Oxide Precursors. *CrystEngComm* **2015**, *17*, 1728−1735.
(38) Reboul, J.; Furukawa, S.; Horike, N.; Tsotsalas, M.; Hirai, K.; Uehara, H.; Kondo, M.; Louvain, N.; Sakata, O.; Kitagawa, S. Mesoscopic Architectures of Porous Coordination Polymers Fabricated by Pseudomorphic Replication. *Nat. Mater.* **2012**, *11*, 717−723.
(39) Okada, K.; Ricco, R.; Tokudome, Y.; Styles, M. J.; Hill, A. J.; Takahashi, M.; Falcaro, P. Copper Conversion into $Cu(OH)_2$ Nanotubes for Positioning $Cu_3(BTC)_2$ MOF Crystals: Controlling the Growth on Flat Plates, 3D Architectures, and as Patterns. *Adv. Funct. Mater.* **2014**, *24*, 1969−1977.
(40) Schmidt, R.; Oh, J. H.; Sun, Y.-S.; Deppisch, M.; Krause, A.-M.; Radacki, K.; Braunschweig, H.; Könemann, M.; Erk, P.; Bao, Z.; Würthner, F. High-Performance Air-Stable N-Channel Organic Thin Film Transistors Based on Halogenated Perylene Bisimide Semiconductors. *J. Am. Chem. Soc.* **2009**, *131*, 6215−6228.
(41) Tan, J. C.; Bennett, T. D.; Cheetham, A. K. Chemical Structure, Network Topology, and Porosity Effects on the Mechanical Properties of Zeolitic Imidazolate Frameworks. *Proc. Natl. Acad. Sci. U. S. A.* **2010**, *107*, 9938−9943.
(42) Cravillon, J.; Schröder, C. A.; Bux, H.; Rothkirch, A.; Caro, J.; Wiebcke, M. Formate Modulated Solvothermal Synthesis of ZIF-8

DOI: 10.1021/acs.chemmater.5b03219
Chem. Mater. 2015, 27, 7673−7679

Investigated Using Time-Resolved in Situ X-Ray Diffraction and Scanning Electron Microscopy. *CrystEngComm* **2012**, *14*, 492−498.
(43) McCarthy, M. C.; Varela-Guerrero, V.; Barnett, G. V.; Jeong, H.-K. Synthesis of Zeolitic Imidazolate Framework Films and Membranes with Controlled Microstructures. *Langmuir* **2010**, *26*, 14636−14641.
(44) Bustamante, E. L.; Fernández, J. L.; Zamaro, J. M. Influence of the Solvent in the Synthesis of Zeolitic Imidazolate Framework-8 (ZIF-8) Nanocrystals at Room Temperature. *J. Colloid Interface Sci.* **2014**, *424*, 37−43.
(45) Schmink, J. R.; Leadbeater, N. E. Microwave Heating as a Tool for Sustainable Chemistry, An Introduction. In *Microwave Heating as a Tool for Sustainable Chemistry*; Leadbeater, N. E., Ed.; CRC Press: Boca Raton, FL, 2010; p 4.
(46) Zhang, X.; Liu, Y.; Li, S.; Kong, L.; Liu, H.; Li, Y.; Han, W.; Yeung, K. L.; Zhu, W.; Yang, W.; Qiu, J. New Membrane Architecture with High Performance: ZIF-8 Membrane Supported on Vertically Aligned ZnO Nanorods for Gas Permeation and Separation. *Chem. Mater.* **2014**, *26*, 1975−1981.
(47) Isaeva, V. I.; Barkova, M. I.; Kustov, L. M.; Syrtsova, D. A.; Efimova, E. A.; Teplyakov, V. V. In Situ Synthesis of Novel ZIF-8 Membranes on Polymeric and Inorganic Supports. *J. Mater. Chem. A* **2015**, *3*, 7469−7476.
(48) Mannsfeld, S. C. B. *WxDiff*; Stanford Synchrotron Radiation Lightsource: Menlo Park, CA, 2009.
(49) Hexemer, A.; Bras, W.; Glossinger, J.; Schaible, E.; Gann, E.; Kirian, R.; MacDowell, A.; Church, M.; Rude, B.; Padmore, H. A SAXS/WAXS/GISAXS Beamline with Multilayer Monochromator. *J. Phys.: Conf. Ser.* **2010**, *247*, 012007.
(50) Ilavsky, J. Nika - Software for 2D Data Reduction. *J. Appl. Crystallogr.* **2012**, *45*, 324−328.
(51) Marcus, M. A.; MacDowell, A. A.; Celestre, R.; Manceau, A.; Miller, T.; Padmore, H. A.; Sublett, R. E. Beamline 10.3.2 at ALS: A Hard X-Ray Microprobe for Environmental and Materials Sciences. *J. Synchrotron Radiat.* **2004**, *11*, 239−247.
(52) Ravel, B.; Newville, M. ATHENA, ARTEMIS, HEPHAESTUS: Data Analysis for X-Ray Absorption Spectroscopy Using IFEFFIT. *J. Synchrotron Radiat.* **2005**, *12*, 537−541.
(53) Cao, S.; Bennett, T. D.; Keen, D. A.; Goodwin, A. L.; Cheetham, A. K. Amorphization of the Prototypical Zeolitic Imidazolate Framework ZIF-8 by Ball-Milling. *Chem. Commun.* **2012**, *48*, 7805−7807.
(54) Roßberg, A.; Reich, T.; Bernhard, G. Complexation of Uranium(VI) with Protocatechuic Acid-Application of Iterative Transformation Factor Analysis to EXAFS Spectroscopy. *Anal. Bioanal. Chem.* **2003**, *376*, 631−638.
(55) Ressler, T.; Wong, J.; Roos, J.; Smith, I. L. Quantitative Speciation of Mn-Bearing Particulates Emitted from Autos Burning (Methylcyclopentadienyl)manganese Tricarbonyl-Added Gasolines Using XANES Spectroscopy. *Environ. Sci. Technol.* **2000**, *34*, 950−958.
(56) Kim, W. B.; Lee, J. S. Quantitative XANES Analysis of Cuprous Dibromide Complex Formed in the Oxidative Carbonylation of Phenols. *J. Phys. Chem. B* **2003**, *107*, 9195−9202.

DOI: 10.1021/acs.chemmater.5b03219
Chem. Mater. 2015, 27, 7673−7679